Translational and Rotational Mobilities of Inclusions Near the Boundary of a Smectic Liquid Crystal Film

By

Ian Cadenhead

Department of Astrophysical and Planetary Sciences

Defense Date: April 4, 2018

Thesis Advisor: Prof. Joseph MacLennan

Department of Physics

Titular Astrophysics Advisor: Prof. Michael Shull

Department of Astrophysical and Planetary Sciences

Honors Council Representative: Prof. Ann-Marie Madigan

Department of Astrophysical and Planetary Sciences

Fourth Reader: Prof. Ian Grooms

Department of Applied Mathematics

Cadenhead, Ian

Translational and Rotational Mobilities of Inclusions Near the Boundary of a Smectic Liquid Crystal Film

Thesis directed by Joseph MacLennan, with Michael Shull as titular advisor

In recent times the properties of quasi-two-dimensional films, similar to biological membranes, have been opened up to experimentation through freely-suspended liquid crystal films. These films, with an extremely thin, quantized thickness, can extend across relatively large distances of up to centimeters, and behave like a fluid in the film plane. The motion of isolated inclusions in these films, described by the inclusion's mobility, is governed by Brownian motion has been extensively modeled and observed. This thesis will examine the behavior of isotropic inclusions near the boundary of a liquid crystal film. This is done by observing three modes of motion: translational motion perpendicular to the boundary, translation parallel to the boundary, and rotation of the inclusion. These observations are then compared to theoretical models of these situations. Our results indicate that mobility perpendicular to the boundary behaves as expected; however, the results for mobility parallel to the boundary are inconclusive, and the results of rotational mobility are greater than theoretical expectations. Future work on this subject includes altering the experimental methods to gather more parallel mobility data, determining the cause for the discrepancy in the rotational mobility, and later extending the experiment to include non-isotropic inclusions.

Acknowledgements

I would like to thank the members of the Liquid Crystal Physics Group, and in particular, I want to recognize those in the Liquid Crystal Films Lab. First, I would like to show my gratitude to Professor Joseph MacLennan for his excellent mentoring and support. To Dr. Cheol Park, thank you for your help and guidance throughout this project. I would also like to thank Adam Green, a graduate student with an outstanding guiding hand. And finally, thanks to everyone else who has supported me during this project.

This research was supported by NASA Grant No. NNX-13AQ81G, and NSF MRSEC Grants No. DMR-0820579 and DMR-1420736.

Contents

Table of Figures

Chapter 1

Introduction

In biological membranes such as cell walls, movement of objects, also known as inclusions, is governed by the process of Brownian motion in a quasi-two-dimensional (2D) fluid. Brownian motion is caused by the random collisions between the fluid particles and the inclusion within the fluid. Diffusion and mobility are two measures used to quantify the motion of an inclusion that account for the random nature of Brownian motion. These two quantities are measures of, respectively, the average distance an embedded object will move in a given time, and the ratio of the object's terminal velocity through the fluid to the force acting on it. Before the 1970's, studies of diffusion were limited to three-dimensional fluids. However, in the mid-1970's P. G. Saffman and M. Delbrȍck developed a theoretical model for diffusion in quasi-2D fluid, which opened up the field to analysis of two-dimensional diffusion [1, 2].

Since then, this theory has been used in many studies of these films, including basic fluid mechanics studies and testing predictions of diffusion and mobility. This includes measuring mobilities of isotropic, or circular, inclusions far from any other object [3], studying the mobility of rod-shaped inclusions [4], and the mechanics that allow liquid crystal films to form [5]. One notable aspect that has not been well studied is the behavior of inclusions near the boundary of a liquid crystal film. A model of this behavior near a boundary can help researchers deal with the real-world case of finite film dimensions, as opposed to the theoretically ideal infinite film case. Such a model could potentially also extend to interactions between two objects of vastly different sizes within a biological membrane.

This thesis will provide a framework of relevant knowledge and research about liquid crystal films, outline the experimental methods I used to test the near-boundary theory, and will compare the theoretical predictions to my experimental results. I will show that translational mobility conforms well to theory, but rotational mobility does not, and make conclusions based on these findings.

1.1 Liquid Crystals

Certain properties of a material dictate how the material behaves on a macroscopic scale, which is encoded in the material's state of matter. The most commonly known states of matter are solids, liquids, gases, and plasma. In general, the differences between these states can be understood as differences in the ordering and motion of the material's constituent particles. For instance, a solid consists of particles that are quite rigidly bound in relation to neighboring particles. In the case of crystals, there is predictable, long-range ordering of the particles in all directions, called a lattice. The particles making up a liquid do not have this long-range ordering, but still retain some short-range ordering and thus remain tightly packed, meaning liquids have a set volume. Gases have no ordering of its particles and they are free to move in all directions, so gasses do not have a definite volume. Plasma, less commonly known than the previous three states, is described as a state more energetic than a gas, and in which particles are ionized.

The term Liquid Crystal (LC) refers to a more recently discovered state of matter that falls between that of the rigid ordering of a solid and the fluid motions of a liquid. There are multiple "degrees", or phases, of liquid crystals. The differences between these phases arises from differences in the positional and orientational order these particles exhibit. These two properties can vary considerably because liquid crystal molecules can take many different forms. Generally, the molecules are rod-like, with one axis longer than the other two. However, there is

variation in this structure: among other possible features, this axis can be bent in one or more places, or the molecule can have a long, flexible tail.

Common liquid crystal phases, shown in Figure 1, include the Nematic phase, Smectic A phase, and Smectic C phase, as well as isotropic, which is another name for the liquid phase, and crystalline, which is the same as the solid phase. The Nematic phase occurs when the molecules are simply orientationally ordered, and are free to move in all directions. The Smectic A phase occurs when the molecules form discrete layers and the molecules orient on average normal to the layer plane, but can still move fluidly within the layer. The Smectic C phase is similar to the Smectic A phase, but the molecules orient at an angle to the layer-plane normal. This orientation causes defects to form in the film, which can alter the hydrodynamics of objects close to them [6].

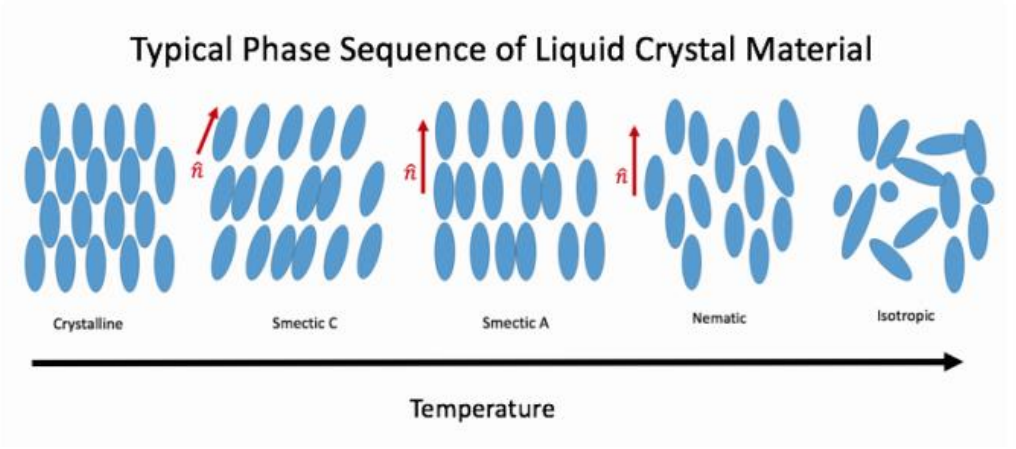

Figure 1: Common liquid crystal phases ordered according to temperature dependence. In the Smectic A, Smectic C, and Nematic phases, $\hat{n}$ indicates the average orientation of the molecules.

Similar to the way most materials transition from solids at lower temperatures to liquids or gasses at higher temperatures, liquid crystals can undergo transitions between different liquid crystal phases with changing temperature. As a fictional example, some material X could

transition from isotropic to nematic at 75°C, from nematic to smectic A at 67°C, and from smectic A to crystalline at 50°C.

A unique feature of smectic liquid crystals is their ability to form extremely thin, freely-suspended films across an opening in a film holder. The film is composed of two or more smectic layers stacked on top of one another. Thus, these films can have a minimum thickness of just a few molecular lengths, which is on the order of tens of nanometers, and still be many centimeters in width. The support for the film comes from the bonds between molecules within the smectic layers. These films are comparable to soap bubbles, but differ in that liquid crystal films have low vapor pressure. The high vapor pressure of the water in soap bubbles causes them to evaporate and burst in a relatively short time; liquid crystal films, conversely, evaporate slowly and are very stable, lasting from hours to days if left undisturbed.

At the edge of the film, the material is connected to the film holder by a meniscus. The meniscus is a region of liquid crystal material that transitions from the film, at tens of nanometers thick, to the thickness of the film holder of roughly a few hundred micrometers (microns). This transition happens over a small span of a few microns, but the large thickness at the film holder compared to the extremely thin film means that most of the liquid crystal material is contained in the meniscus. The meniscus is thought to be structured similar to the film itself, with layers stacking on top of one another and all enclosed within the outer layers, as depicted in Figure 2.

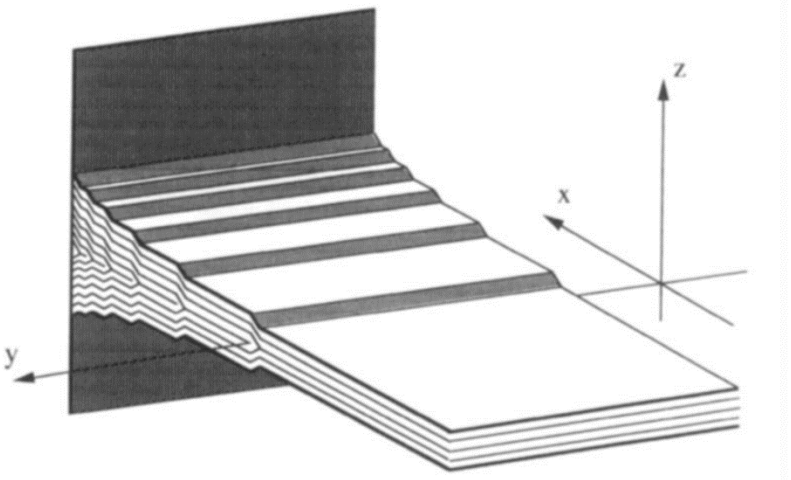

Figure 2: Proposed structure of meniscus, with the number of layers and thickness increasing drastically near the film holder [5].

The meniscus also serves as a reservoir of liquid crystal for the rest of the film to draw material from in order to account for volume changes due to events in the film.

A smectic liquid crystal film does not always have a uniform thickness throughout. Often, after a film is drawn there will be some large areas that have more layers than others. Layer steps can fluidly move about and interact with inclusions in the film in undesired ways. This can be remedied by simply waiting for some time after the creation of the film. The "extra" material in these layers will be drawn into the meniscus, and the film will be uniform and have the thickness of the thinnest initial area.

1.1.1 Islands

A different manifestation of extra material in the film is a small, disk-shaped region of greater thickness called an island. These islands are generally quite small compared to the film itself, having radii between several microns to a couple of hundred microns. These islands are generally stable and can last several tens of minutes, as compared to the initial large regions of different thickness that are absorbed into the meniscus within about a minute. This is because the larger regions are connected to the meniscus, and the excess material gets drawn into the meniscus. Islands are disconnected from the meniscus, and thus cannot undergo the same process unless they touch the meniscus, a process that will be discussed later. Islands do slowly shrink over time, though this process is not well understood. It is believed that the shrinking is caused by the diffusion of molecules from one layer in the film to another; over time, material in the island will be transferred to the film surrounding it. This process is very slow compared to the diffusion of molecules within a layer.

The precise structure of an island is not conclusively known. The prominent theory is that the extra layers are squeezed between the smectic layers of the surrounding film, as depicted in

Figure 3. Another option is to have the excess material sit on top of the film. Both of these models require an edge dislocation in the layers at the boundary of the island that requires free energy to maintain. The shrinking of the island happens to minimize and eventually eliminate this edge dislocation, lowering the free energy.

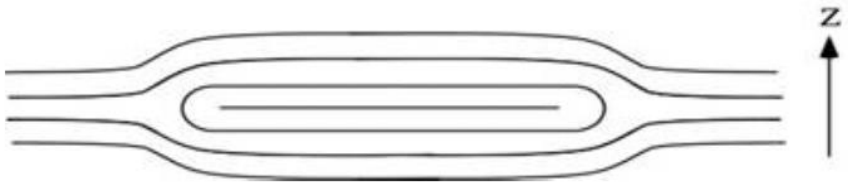

Figure 3: Cross-section of a liquid crystal island, showing the extra layers encased in the film layers.

Islands can be formed in a few ways. Sometimes islands will have formed spontaneously upon drawing a film, due to small isolated areas of increased thickness, but this is rare and entirely random. The most common method of creating islands it to draw extra material out of the meniscus onto the film. This can be done by gently blowing air across the meniscus, using compressed air or blowing through a straw, to draw material from it onto the film. This method requires some practice, as it can be hard to precisely control the force, and blowing too hard may pop the film. An alternative is to deposit particles, such as dust or ash, onto the film. These particles serve as a nucleus for an island to grow around, and because these particles are generally much bigger than the film is thick, they allow easy transport of material between layers. This method is also imprecise, as there is no way to control the number of particles that generate islands, and depositing ash particles can also sometimes pop the film. Other methods of precise island generation are currently being explored, such as using an inkjet printer, but have not yet been perfected.

Island-island coalescence can happen if two islands come in contact. This process is similar to island absorption into the meniscus, but has distinct features as well. In a coalescence event, the corresponding smectic layers merge almost immediately, and the new, merged island to re-form into a circular disk very rapidly. The extra material in each of the resulting layers results in a new island with a radius larger than the two contributing islands.

If the two contributing islands are not the same thickness, then an additional stage happens after the initial coalescence. At this point, the layers that were present in both initial islands have combined to form larger disks, but there are one or more layers that did not gain additional material and cannot fill the same area, resulting in an island on top of another island. However, this smaller island draws material from the other layers of the merged island and grows while the other layers shrink. This continues until all layers in the merged island have the same radius. The result is a single, uniform island that is the thickness of the thickest initial island, but may not be larger, or even have the same radius, as either initial island.

Finally, when an island touches the meniscus, it is absorbed almost instantaneously. This is much like island coalescence, as every layer of the island is matched by one of the layers in the meniscus, but the island is completely absorbed into the meniscus without changing the meniscus geometry very much. This is because the meniscus is a reservoir of material, and the material from the island is relatively insignificant.

1.1.2 Properties of 8CB

The liquid crystal used in the experimentation for this thesis is known as 4′-n-octyl-4-cyano-biphenyl (8CB), and its chemical diagram is presented in Figure 4. The “8” in 8CB refers to the number of carbon atoms in the alkyl “tail”. The “C” represents the cyano head group and the “B” represents the biphenyl rings, the combination of which make up the molecule. This

molecule is attractive to use for studying two-dimensional diffusion. One reason is that the basic properties of the 8CB molecule are well known, allowing researchers to avoid measuring these for themselves. Another important reason is that 8CB is in the smectic A phase at room

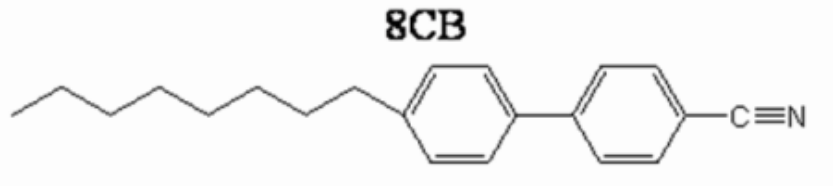

Figure 4: Chemical structure of 8CB.

temperature, which allows films to be created without complex temperature controlling systems. Finally, the price of 8CB has reduced drastically since its discovery, making it one of the least expensive liquid crystal materials available.

As mentioned, numerous studies have explored the properties of the 8CB molecule. The length of the molecule, which is also the thickness of the smectic layers it forms, is 3.17 nm [7]. In bulk, the density of 8CB is $\rho \approx 0.96$ g/cm [8]. When at room temperature T = 22°C, 8CB has a viscosity $\eta_{8\mathrm{CB}} = 0.052$ Pa $\cdot\, s$ [9], while the viscosity of the surrounding air is $\eta_{\mathrm{air}} = 1.827 \times 10^{-5}$ Pa $\cdot\, s$ [10]. Another important property, the index of refraction, is $n_{8\mathrm{CB}} = 1.516$ [11]. 8CB has only two liquid crystal phases. Above 41°C, 8CB is isotropic. Between 34-41°C 8CB is in the nematic phase, between 20-34°C it exists in the Smectic A phase, and below 20°C 8CB is crystalline.

Chapter 2

Theoretical Background

The diffusion of an isotropic inclusion in a quasi-2D fluid has been extensively studied and is well understood, including both translational diffusion and rotational diffusion [3, 12]. This Thesis explores the effect that an inclusion's proximity to the film boundary has on its mobility. Three different cases are covered: translational diffusion parallel to the boundary, translational diffusion perpendicular to the boundary, and rotational diffusion.

2.1 Diffusion of an Isolated Inclusion

Brownian motion was first observed by Robert Brown in 1827 while he was examining amyloplasts, or starch organelles, in water [13]. This discovery sparked debate on the nature of matter; it was thought that only living organisms would exhibit such random, active behavior. This new finding lead to two revised theories of the composition of matter: that it was composed of fundamental particles, and that it was pure energy. This debate was settled in 1905 when Einstein proved that matter is composed of atoms [14]. Einstein, simultaneously with Marian von Smoluchowski [15], proposed that Brownian motion is caused by random interactions between the fundamental particles making up the fluid and the embedded object.

To quantitatively analyze the motion of particles, the concept of diffusion was created. The diffusion law states that for a particle undergoing a random walk, the particle will have some average displacement that is a function of the time it spends diffusing. The average squared displacement per unit time is called the particle's diffusion coefficient. In one dimension, the diffusion coefficient may be calculated using the mean-square-displacement (MSD) of the particle, described in equation 1:

$$\langle r^2 \rangle = 2Dt \, , \tag{1}$$

where D is the diffusion coefficient, t is the time the particle is tracked, and $\langle r^2 \rangle$ is the MSD of the particle for this track. For isotropic diffusion in two dimensions, it is possible to simply add the two one-dimensional diffusion coefficients:

$$\langle r^2 \rangle = \langle x^2 + \, y^2 \rangle \, = 2 \, Dt + \, 2 \, Dt = 4 \, Dt \, . \tag{2}$$

The translational mobility of a particle μ is defined as the ratio of the drift velocity of the particle to the force on the particle causing that drift,

$$\mu = \frac{v_d}{F} \, . \tag{3}$$

When the force on the particle is known, this calculation is trivial. However, the force due to Brownian motion is quite complicated, and depends on properties of the fluid and the geometry of the particle. If the diffusion coefficient is known, then the mobility can be calculated using

$$D = \mu k_B T, \tag{4}$$

where T is the temperature of the film in Kelvin and k_B is Boltzmann's constant.

2.1.1 Translational Diffusion

In the case of an inclusion in a Smectic film, the particle will typically extend out of the film and into the surrounding fluid (in this case air). The air will therefore affect the particle through Brownian mechanics, which must be accounted for too. To deal with this situation of one two-dimensional fluid bounded by a second fluid, there is a characteristic length scale set by the viscosities of the two media, called the Saffman length l_s [1]:

$$l_s = \frac{n_{2D}}{\eta_{surround}} = \frac{h_{film} \, \eta_{8CB}}{2 \, \eta_{air}} \, . \tag{5}$$

In equation 5, the two-dimensional viscosity n_{2D} is the bulk viscosity of 8CB, η_{8CB}, multiplied by the thickness of the film h; the viscosity of the surrounding medium, $\eta_{surround}$, must account for the media both above and below the film, which in our case is air, so $\eta_{surround}$ is equivalent to 2 η_{air}. For cylindrical particles with sizes much smaller than the Saffman length, the translational mobility is independent of the amount the particle extends into the air, and it is possible to calculate the mobility using equation 6:

$$\mu = \frac{1}{(4\,\pi\,\eta_{8CB}\,h_{film})}\left(ln\left(\frac{l_s}{a} - \gamma\right)\right), \tag{6}$$

where a is the radius of the particle and γ is Euler's constant, $\gamma = 0.577215$ [12]. The result of this equation is that when a << l_s, the particle's mobility depends on the viscosity of the film and the thickness of the film, and the two-dimensional radius of the particle.

When a >> l_s, the mobility of the particle asymptotically approaches the three-dimensional behavior. This is modeled [16] by the equation

$$\mu = \frac{1}{16\,\eta_{air}\,R}. \tag{7}$$

This is very similar to Stokes' Law [17] for a spherical particle in a three-dimensional fluid:

$$\mu = \frac{1}{6\pi\eta R}. \tag{8}$$

This is a surprising result, but is explained if the outer edge of the particle is coupled to the surrounding air. In this case, the particle will be dragging a bubble of air with it as it moves that turns this into an inclusion embedded in a 3-dimensional fluid but confined to diffusing in 2 dimensions.

The case where the radius is on the order of the Saffman length is much more complicated than the two extreme cases. There are two extremely important contributions to the solution for mobility in this region. First, a representation of this region using infinite spherical Bessel functions by B. Hughes, B. Pailthorpe, and L. White, (HPW) [16]. This method is an excellent approximation, but is computationally intensive and thus undesirable when quick analysis is needed. Second, an analytical approximation based on a fit to the HPW solution devised by E. Petrov and P. Schwille [18], shown in equation 9:

$$\mu = \frac{1}{(4\,\pi\,\eta_{8CB}\,h_{film})}\left(\frac{ln\left(\frac{2}{\varepsilon}\right)-\gamma+\frac{4\varepsilon}{\pi}-\left(\frac{\varepsilon^2}{2}\right)ln\left(\frac{2}{\varepsilon}\right)}{1-\left(\frac{\varepsilon^3}{\pi}\right)ln\left(\frac{2}{\varepsilon}\right)+\frac{c_1\varepsilon^{b_1}}{1+c_2\varepsilon^{b_2}}}\right). \tag{9}$$

In the above equation, ε is the reduced radius a/l_s, and there are four fitting parameters: b_1 = 2.74819, b_2 = 0.51465, c_1 = 0.73761, and c_2 = 0.52119. Petrov and Schwille report that this fit has a relative error below 0.015% when compared to the HPW for all ε [18]. Figure 5 contains a logarithmic plot of the Petrov-Schwille approximation for a large range of reduced radii ε, as well as the two-dimensional and three-dimensional asymptotic limits.

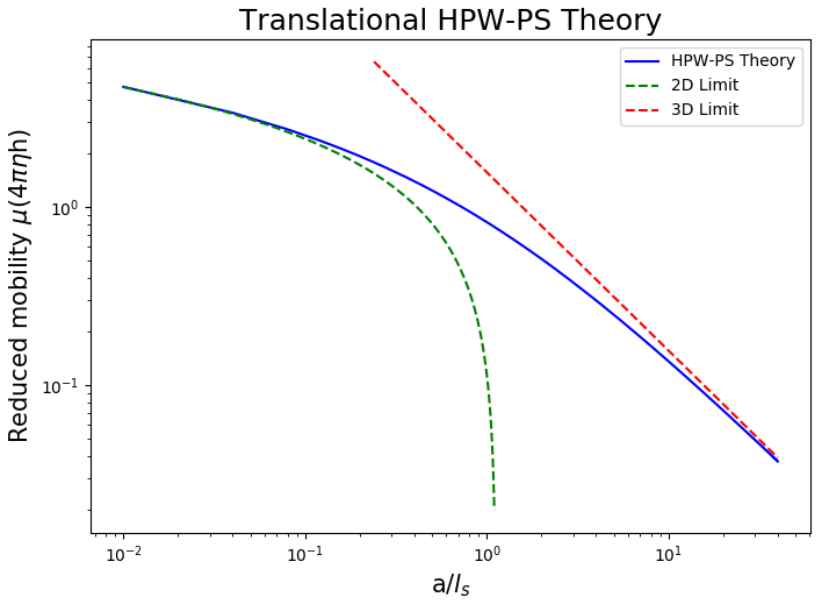

Figure 5: Translational HPW-PS theory curve for values of ε=a/l_s between the 2D and 3D asymptotic limits.

2.1.2 Rotational Mobility

The rotational mobility has a similar theory. Just as in the translational case, the HPW group found a solution by solving an infinite system of linear equations [16]. Once again, the computationally intensive nature of this solution led the group Eugene P. Petrov, Rafayel Petrosyan and Petra Schwille to develop a simple numerical approximation [12]. The function this group used to approximate rotational mobility is

$$D_R = \frac{k_B T (2\eta_{air})^2}{4\pi (h\eta_{8CB})^3} \left[\varepsilon^2 + \frac{4\varepsilon^3}{3\pi} + \frac{c_{R1}\varepsilon^{b_{R1}}}{1 + c_{R2}\varepsilon^{b_{R2}}} \right]^{-1}, \tag{10}$$

where $b_{R1} = 2.91587$, $b_{R2} = 0.68319$, $c_{R1} = 0.31943$, and $c_{R2} = 0.60737$. This function is reported to have a relative error below 0.07% over the whole range of ε.

Both of these approximations are very good for inclusions in the bulk of the fluid, far from the boundary. However, at the boundary it is expected that there is a no-slip condition. This means that the fluid in contact with the boundary is strongly coupled to the boundary itself and will not have any significant motion. This means that there is a transition from the bulk-value mobility for inclusions far from the boundary to zero mobility when the inclusions are in contact with the boundary.

Modeling this transition is no easy task; the boundary effects are not linear, so making any calculations requires solving large numbers of equations. The method used for the theory I am testing against makes use of work done by Levine and MacKintosh, who developed a method of calculating the displacement response of a fluid at a given point by summing the point-like forces acting from all other points in the fluid [19]. This theory was then adapted to provide a velocity response at any point in the membrane [20].

2.2 Model Near a Boundary

To calculate the mobility of an extended inclusion, a large number of these point forces, called Levineslets, can be rigidly arranged in the shape of the inclusion. The velocity response can then be calculated at any point in the membrane by summing the contributions from each point force. To determine the inclusion's mobility, this response is calculated at each point in the membrane surrounding the object, creating a velocity field. From this velocity field an overall velocity can be extracted (assuming the points making up the object are fixed relative to one-another). This method has been used to calculate the translational and rotational mobility of extended rod-shaped inclusions embedded in a two-dimensional fluid [4,20].

The specific numerical implementation of the Levine/MacKintosh theory used for this experiment was developed by Tatiana Kuriabova and Thomas Powers for circular inclusions. This method takes the radius of the island as an input, then places Levineslets along the film

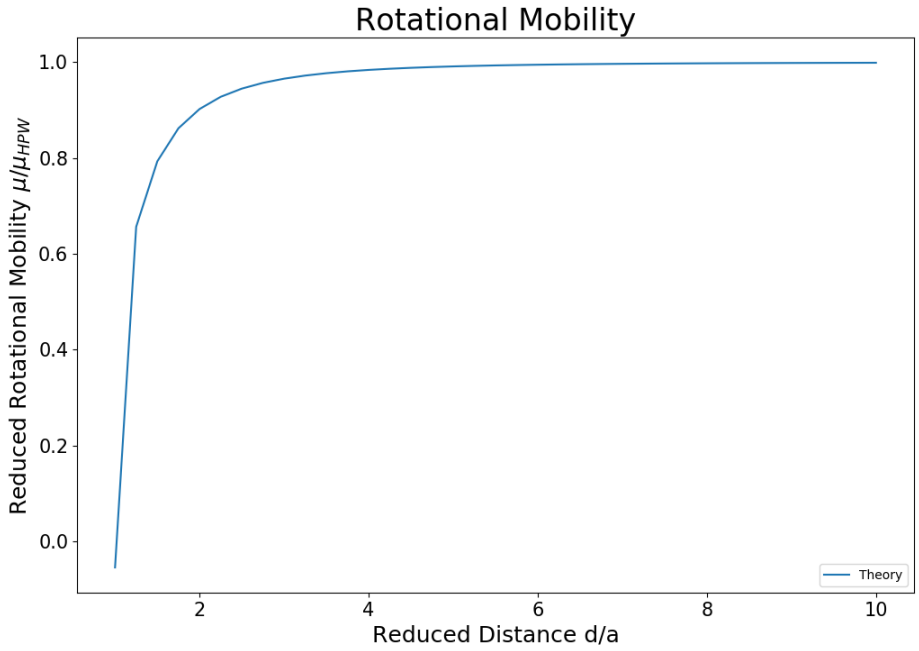

Figure 6: Theoretical rotational mobility as a function of distance. On the x-axis, d is the shortest distance between the island's center and the film boundary, and is converted into a unitless reduced quantity by dividing it by the island's radius a. On the y-axis, the reduced mobility is defined as the ratio of the calculated mobility μ to the bulk HPW prediction of mobility μ_{HPW}. In this figure, $a / l_s = 0.5$.

boundary and within the island [21]. These Levineslets are used to calculate the velocity field in an area around the island, from which velocity and rotation are calculated for the island at varying distances separating the boundary and the island's center. The result is a mobility that depends logarithmically on the island's distance from the film boundary, such as that shown in Figure 6.

Chapter 3

Experimental Methods

3.1 Apparatus

Experiments were conducted using a Nikon Optiphot microscope, a reflected light microscope with an incandescent lamp light source, shown in Figure 7. Attached to the microscope is a CCD camera to record images and video. The incoming light can be diverted to either the eyepiece or the camera by simply rotating the eyepiece. The microscope is equipped with a turret to allow easy switching between objectives. For this experiment 5x, 10x, and 20x objectives were used.

Figure 7: Nikon Optiphot Microscope and Goniometer. The microscope has a Watec camera mounted on the top and an incandescent light source mounted on the arm to the left. The entire microscope is attached to a goniometer, seen at the rear of the microscope.

This microscope is mounted on a Goniometer that allows the entire microscope to be tilted on one axis. This is done through a series of gears driven by a hand crank on one side. The tilt angle can be measured accurately to within a couple of arcminutes (accounting for slop in the gears). This is visually represented by degree markings on the main mount, shown in Figure 8-a, and arcminute markings on the hand crank, shown in Figure 8-b.

There are 240 markings on the handle, so one full rotation of the hand crank rotates the microscope by 4 degrees. To find the goniometer setting at which the microscope is level, we

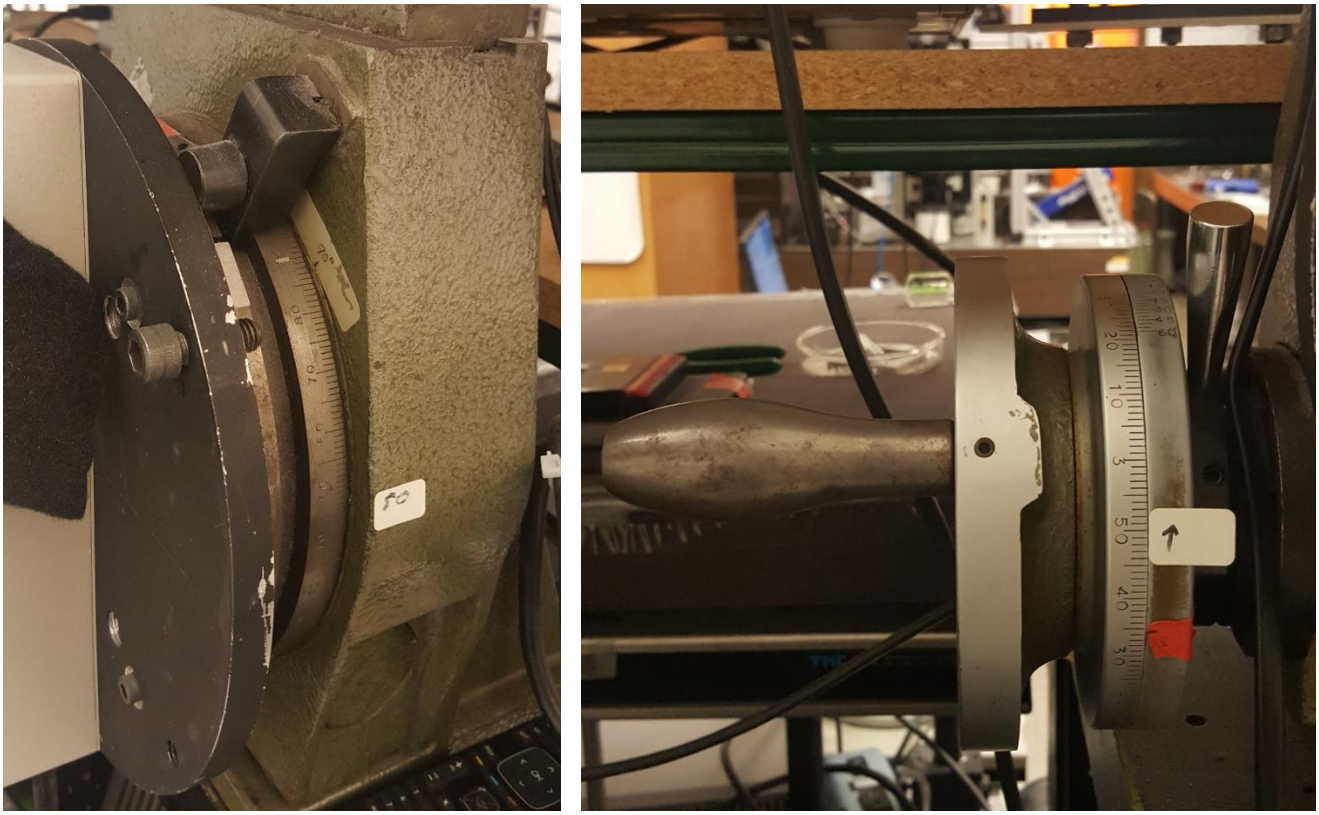

Figure 8: (a): Tick marks on the main section of the goniometer that indicate angle in degrees. (b): Hand crank to the left of the microscope, which has tick marks that denote the angle in arcminutes.

measured the drift velocity of a single particle foe a number of tilt angles around the expected leveled angle, then regressed these velocities to zero on a plot of velocity vs. tilt angle.

The addition of the goniometer allows the tilting of the microscope stage while keeping the objective perpendicular to the sample. This gives us the ability to precisely manipulate islands in the film along the x-axis using the force of gravity. This is a reasonably efficient, low-tech alternative to other manipulation techniques such as optical tweezers.

The CCD camera mounted on the microscope is a Watec video camera, the WAT-221S. This camera records video at 30 frames per second at a resolution of 640 x 480 pixels. One

benefit of this camera is the ability to change the shutter speed, and thus exposure time. This is important in getting calibrations for measuring film thickness, as discussed in Chapter 3.2.

Finally, there is the film holder and its stage. The film holder consists of a glass cover slip with a rectangular hole cut out in the center, shown in Figure 9-a. This cover slip is attached to a metal frame that can be mounted on a hot stage, as shown in Figure 9-b. This stage has two micrometers for linear translation in the x- and y- directions that allow finely controlled movement of the film holder across the microscope's focus. The rectangular (rather than circular) hole geometry was chosen specifically to give straight, well-defined boundaries for the film. This minimizes any difficulty in measuring island distance from the boundary, and creates well-defined parallel and perpendicular directions relative to the boundary.

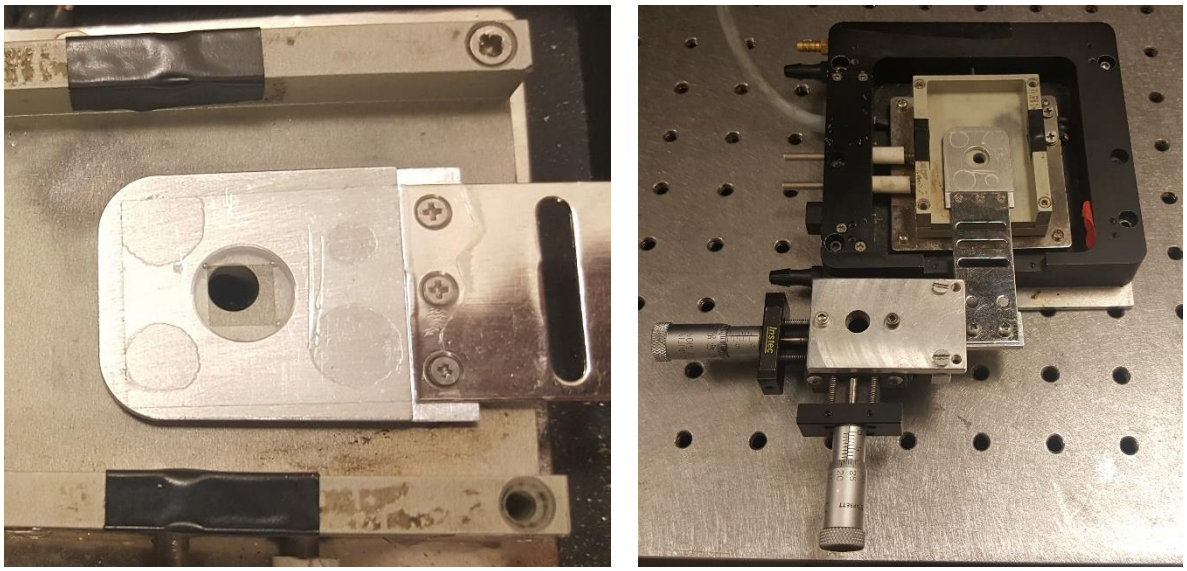

Figure 9: (a): Glass film holder with a square hole cut in the center, mounted on two aluminum parts. (b): Film holder and mount attached to a hot stage, with two linear translation screws for fine adjustments to the film holder's position.

To protect the film from air currents in the room that can adversely affect the motion of the islands, we have made a special air shield that fits on the stage, covering the film holder and minimizing gaps for stray air flows to enter the "chamber." This shield is constructed from 3D printed plastic, designed using SolidWorks to fit snugly around the lip of the hot stage as

depicted in Figure 10. Additional “brushes” were also added to the front of the shield, where the metal frame passes through to attach to the translation screws. These flexible brushes, made from electrical tape with slits cut out, further minimize any openings into the chamber without inhibiting the translation of the film holder.

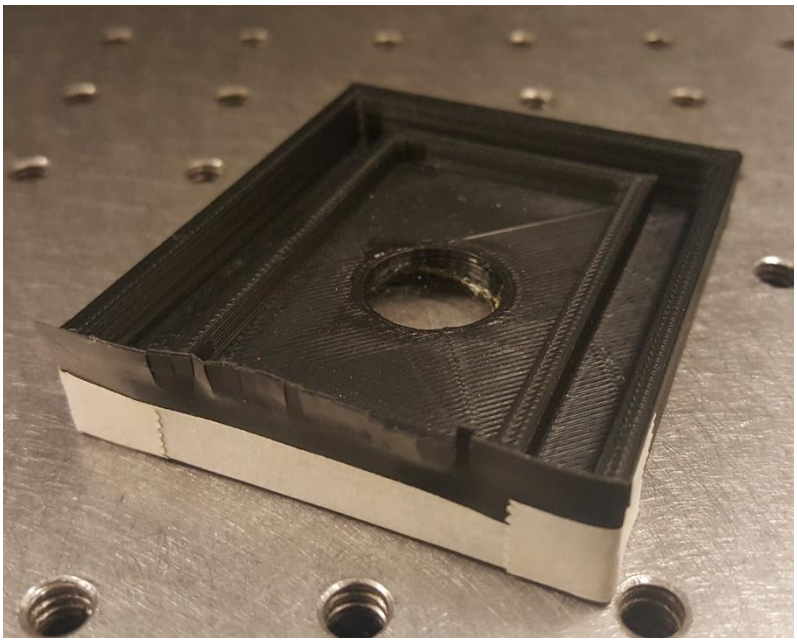

Figure 10: View of the bottom of the film shield, designed to match the hot stage around the film holder. In the center is an angled glass window to minimize reflections and air flow.

3.2 Measuring Thickness

The thickness of the film and the island are necessary for calculating many properties, such as the viscosity of the film or the mass of the island. This is determined by the intensity, and potentially the color, of the light reflected off the film. This intensity is affected by the interference between the light reflected from the top of the film and the light reflected from the bottom of the film. The intensity of the white light reflection is proportional to the thickness of the film squared for films less than ~20 layers thick. For films greater than about 20 layers in thickness, the reflectivity depends on wavelength, overall color changes, and the intensity no longer follows the simple function below. This can be adjusted for by using the Michel-Lévy

Interference Color Chart, shown in Figure 11. This is difficult to accurately use, and thus we try to avoid extremely thick films or islands when precise thickness measurements are necessary.

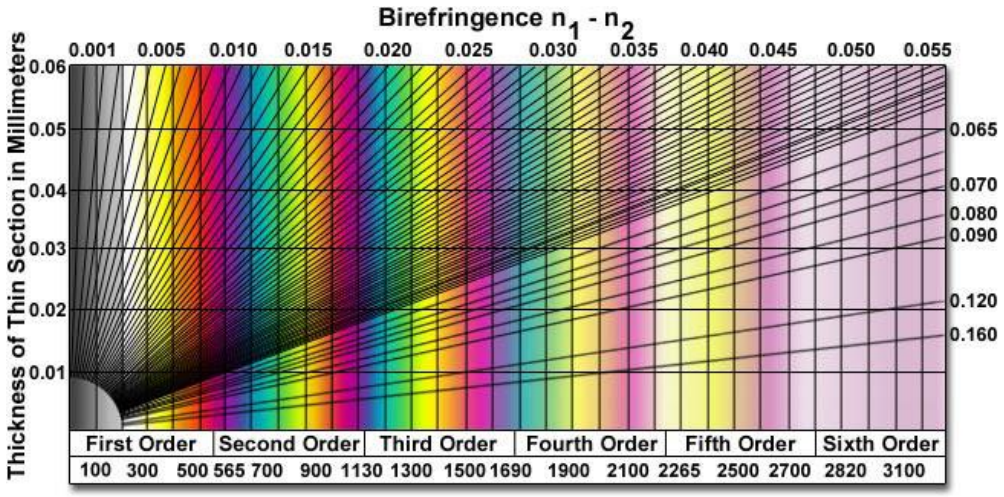

Figure 11: Michel-Lévy interference color chart. By using the color of the island or film and the birefringence, this chart can be used to determine the thickness of the sample.

In this experiment, both the incident and reflected light are normal to the air-8CB interface. This means that the reflectance from an air-8CB interface only depends on the index of refraction of the two media:

$$r = \frac{n_{air} - n_{8CB}}{n_{air} + n_{8CB}} = \frac{1 - 1.516}{1 + 1.516} = -0.205\ . \qquad (11)$$

The value $n_{8CB} = 1.516$ is the index of refraction for the short axes of the 8CB molecule. This is because 8CB films are in the Smectic A phase, so on average the molecules are oriented normal to the layer plane, and the long axis is not sampled by the light incident normal to the layers.

The interference of the reflected light arises from the phase difference between the light reflected off the top and that reflected from the bottom. As the reflection off the top happens with the light going from low- to high- index of refraction, this ray acquires a phase shift of 180°, or π radians. The ray that reflects off the bottom of the film is going from high- to low- index of refraction, so does not experience this effect. However, this ray must travel both down and back

along the thickness of the film, causing a difference of path length between this ray and the one reflected off the top that does add a phase difference for this ray. This, combined with the shortened wavelength of the light as it travels through the liquid crystal, is called the retardance, and is represented by the formula

$$\beta = \frac{2\pi nNa}{\lambda}, \tag{12}$$

where n is the index of refraction, λ is the wavelength of incoming light, N is the number of smectic layers, and a is the length of the molecule (N*a = h, the distance travelled in one direction through the film).

In this experiment we deal mostly with films and islands in the < 20-layer range. In this case, the film reflectivity can by modeled by the following equation using r and β [22]:

$$R = \frac{2r^2(1-cos(2\beta))}{1-2r^2\,cos(2\beta)+r^4}. \tag{13}$$

This equation gives the expected intensity of reflected light for a given reflectance r and retardance β. By choosing a specific wavelength λ to work with, such as 510 nm, then varying the film thickness N, it is possible to calculate the expected reflected intensity for a range of film thicknesses at that wavelength.

The next step was to gather calibration data to compare a sample thickness measurement against. To do this, I drew many films of varying thickness, then took snapshots of the film using the Watec camera at four different shutter speeds: 1/60 s, 1/100 s, 1/250 s, and 1/500 s. I then extracted intensities for one color channel (usually green), and found the average intensity of the film at each of these exposure times. From these data, I computed a best-fit slope of intensity vs. exposure time for each film, as depicted in Figure 12. As the figure shows, the slopes will form clusters that include films with the same thickness. By taking the average of each of these

clusters of slopes, I could calculate the expected intensity for each (unknown) film thickness. I then took either the cluster with the smallest slope or the second smallest slope, and used it as a

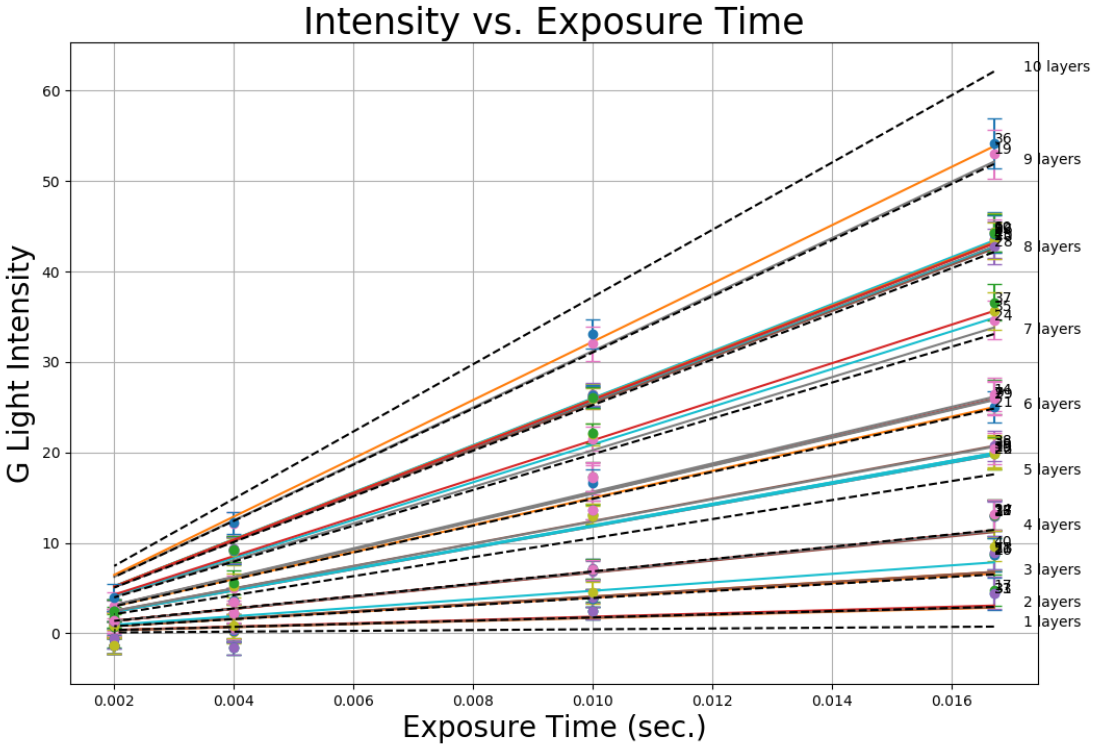

Figure 12: Plot of green light intensity for a number of sample films at different exposure times, and their best-fit lines. The dashed lines indicate the theoretical intensity predicted for each thickness.

"reference thickness": I guessed the thickness of this cluster, and assign it this thickness. Then, I paired the reflectance calculated for that thickness with the measured intensity of this cluster. This means I could simply multiply the reflectance calculated for other thicknesses by the ratio of sample intensity to the sample reflectance. This creates a set of expected intensity slopes to which I could compare the rest of the measured data. I repeated this process until I found a thickness for the given cluster that generated other intensity slopes that matched the rest of the clusters, seen as the dashed lines in Figure 12.

This means that the dependence of intensity on exposure time is known for each film thickness; I can then use this to calculate the expected intensity of any thickness of film for a

given value of the exposure time, say 1/30 s. These values can then be saved into a spreadsheet to quickly reference against experimental measurements of intensity at this exposure time.

3.3 Experimental Setup and Data Collection

To conduct the experiment, an 8CB film must first be prepared. The process of creating, or "drawing" a film is fairly simple. A small amount of 8CB material is placed on the edge of a glass cover slip, which is called the spreader. The edge of the spreader is then drawn across the opening of the film holder. When drawn at a specific angle and with a certain amount of pressure between the spreader and film holder, a thin film of material is stretched across the opening in the film holder as depicted in Figure 13. Unfortunately, the success of this process is random, and it must generally be repeated several times before a stable film is created in the film holder.

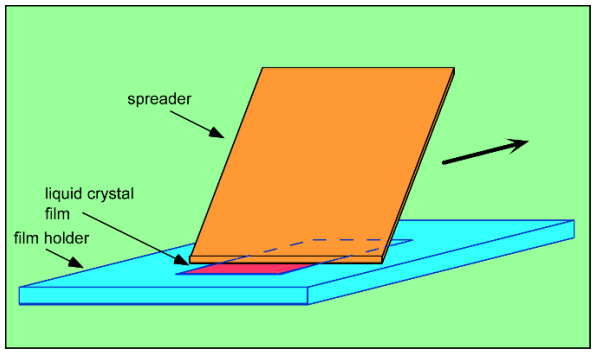

Figure 13: Depiction of a film being drawn across an opening in the film holder by the spreader.

As discussed in Chapter 1.1, there are often regions of differing thickness in the film after a film is drawn. These non-uniformities can cause unwanted hydrodynamic effects on the system, so the film is allowed to sit, letting the thickness become uniform. In most cases, after a few minutes the excess material is drawn into the meniscus, but sometimes these regions form islands. If islands do not form spontaneously, or if they do form but are too small/too large for the video camera to detect, then islands are actively created by blowing on the film, as discussed in Chapter 1.1.1. This is done until either the film pops or islands of the desired size are created.

If rotation is being tracked, an additional step is necessary. Islands are isotropic circular objects with no visible features to indicate orientation. To create such features, it is possible to deposit particles onto the film that create reference points on the film and in the islands. This is done with ash particles: incense smoke is collected in a downward-facing jar, which is then placed over the film. The ash particles will then settle onto the film.

To avoid island-island hydrodynamic interactions, tracked islands must be "isolated" from one another. In practice, this means they must be separated by several Saffman lengths. This ensures that the "Saffman clouds" of the islands do not interact (or only interact weakly), so effects from other islands are small compared to the effects due to the film itself. Unwanted islands can be eliminated by tilting the film so that the flow to the meniscus, where they are absorbed.

Once a desired island is created and isolated, there are three modes of motion that I characterize: translational motion perpendicular to the boundary, translational motion parallel to the boundary, and rotational motion, as depicted in Figure 14.

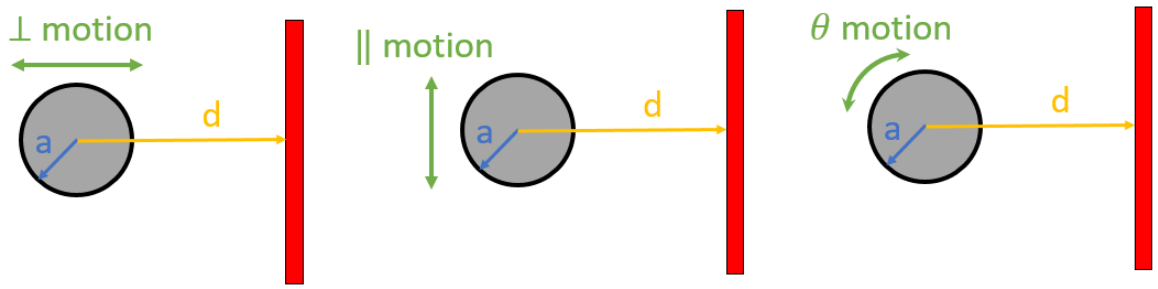

Figure 14: Cartoon representations of the three modes of diffusive motion.

To measure translational mobility perpendicular- and parallel- to the boundary, I make use of the goniometer. As shown in equation 3, the mobility of an object depends on the force

acting on the object and the object's terminal velocity due to this force. By tilting the microscope with the goniometer, a gravitational force is imparted on an island; if the mass of the island and the tilt angle are known, then the gravitational force can be calculated. Then, because the island is moving through a fluid, viscous drag will cause the island to reach terminal velocity, which can be measured. With these two quantities known, the mobility can be easily calculated.

The angle of tilt is straightforward to determine using the method discussed in Chapter 3.1. The mass of the island is somewhat more difficult to calculate. This requires the density of the material, which is known, and the volume of the island. The island is a cylinder, so its volume requires the radius and the thickness of the island. The radius is simple to determine, as the scale factor from pixels to micrometers in recorded video is calculated using a graticule. The thickness is determined as outlined in Chapter 3.2. However, this thickness also includes the film that the island is embedded in. Therefore, the thickness of the film must be subtracted from the measured thickness of the island to find the thickness of the portion of the island that is affected by gravity.

The goniometer can only tilt the microscope about one axis, so to select for parallel or perpendicular the hot stage is simply rotated by 90°. Then, the microscope is tilted to an angle that causes the motion due to gravity to be the dominant factor, much larger than the Brownian motion. To keep the experiment as simple as possible, I have limited the motion to purely parallel or perpendicular to the film boundary. This is done to avoid any unforeseen effects when mixing parallel and perpendicular motion. However, this method has its own limitations, discussed further in Chapter 5.2.

When measuring rotational mobility, the island was kept as stationary as possible, or was given a very slight drift toward or away from the boundary. This is again an effort to minimize

any effects that translational motion might have on the rotation. It is particularly important to minimize the parallel motion: the effect that is thought to cause the logarithmic behavior of the mobility near the boundary is a gradient in the fluid pressure. This is caused by the boundary preventing fluid molecules from moving out of the way of the island. However, a slight drift perpendicular to the boundary facilitates taking mobility measurements at different distances in a shorter amount of time.

Chapter 4

Data Analysis

4.1 Island Tracking

After video is recorded, the individual video frames are used to track the island (and ash particles if present), then either calculate the instantaneous velocity or calculate the mean-square-displacement of the island for different time-lags. These results are then converted into mobilities, and plotted against the reduced distance from the boundary to the island. Another program, written in MATLAB by Professor Tatiana Kuriabova, is used to numerically calculate the theoretical mobility expectation for a range of distances using Levineslet point forces.

The video is decomposed into an image stack which is then passed into an IDL program, written by Professor Joseph Maclennan, that tracks the particle's position, shape, and distance from the film boundary. This program takes the framerate and pixel-to-micrometer conversion factor as inputs, as well as allowing image processing such as binary thresholding. Then, a seed coordinate that falls within the island is passed; from this seed the program grows a region of pixels with similar intensities until it finds a border. For an island, a circle is fitted to the boundary of this region, and values such as the radius and the coordinates of the island's center are saved. The edge of the meniscus closest to the island is approximated by a straight line, and the shortest distance between this edge and the island's center is found. The program will repeat this process for each image, using the calculated center of mass of each region as the seed coordinate in the next frame. Once the program has finished, it saves the data to files.

4.2 Particle Tracking

Tracking smaller particles, such as the ash particles used to measure orientation, poses a problem to this program. Often, the particle is quite small and will move a considerable amount

in one frame of video, and the track is immediately lost. To track these particles, I use another program written by Professor Maclennan, which is based off work by John Crocker and Eric Weeks [23]. This program measures the position of all particles that fall within certain specifications, like size or intensity, and will use algorithms to determine how to connect tracked points between frames.

4.3 Analysis

Once the objects of interest have been tracked, I use Python programs that I have written to do the remaining analysis of mobility. In the case of translational motion, this is as simple as using Δx and Δt at each frame to determine the velocity the island is moving at in each frame, calculating the force of gravity, and taking the ratio of these to find the mobility. To simplify the results, this mobility is then divided by the mobility expected if there was no boundary present, μ_{HPW}, found using equation 9. This results in a dimensionless fractional mobility, $\frac{\mu}{\mu_{HPW}}$.

For the case of rotational motion, I have written a Python program based around the particle tracking library Trackpy. This program can take in an array of times and an array of the angular orientation at these times, and will calculate the mean-square-displacement and its error as a function of the time between samplings, called the lagtime. This results in a plot like that in Figure 15. Then, a weighted fit is taken of these points to find the slope. Using equation 1, this slope $\left(\frac{\langle\theta^2\rangle}{t}\right)$ is divided by two to find the rotational diffusion coefficient of the island, which is related to its rotational mobility by equation 4. Again, this is transformed into a dimensionless fractional mobility by dividing it by the expected rotational mobility with no boundary, done by finding $D_{R,0}$ using equation 10 and converting this into a mobility.

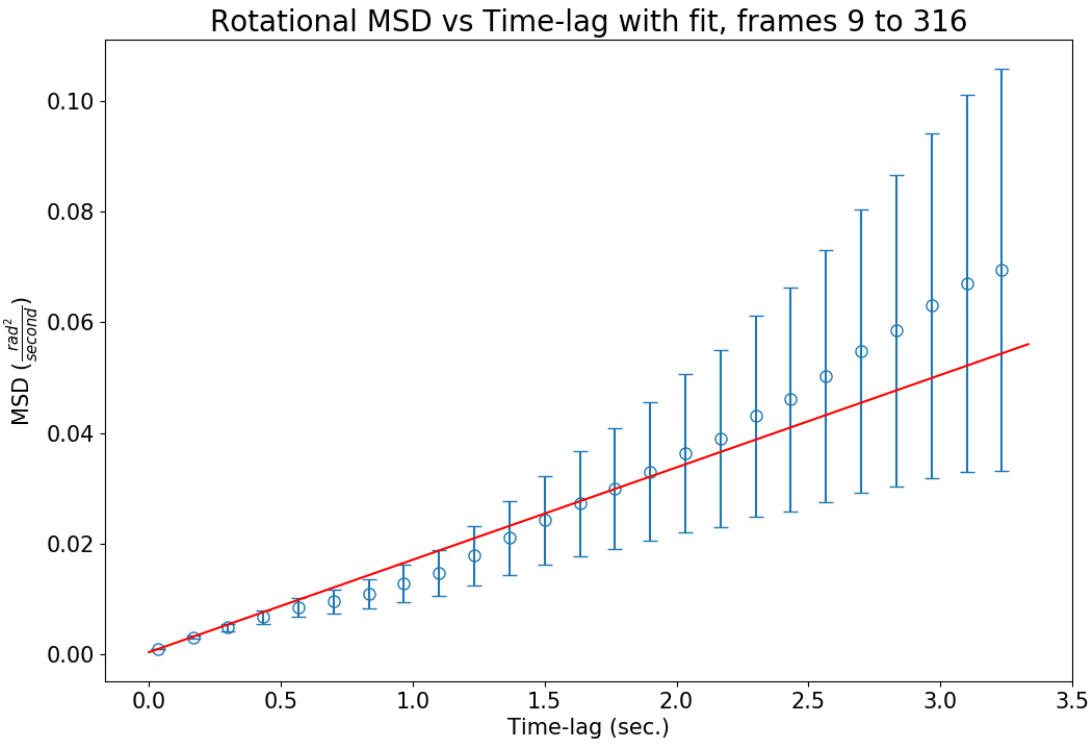

Figure 15: Example of an MSD plot over a range of small lagtimes, and a weighted best-fit line. This plot was created from a data set of 307 frames, calculating the angular MSD for lagtimes up to and including 100 frames. Using the best-fit line, the measured rotational diffusion coefficient for this data set is $(8.33 \pm 0.38) \times 10^{-3} \ \frac{(radian)^2}{s}$.

Chapter 5

Results and Discussion

The results of this analysis are mixed. The perpendicular translational mode shows good agreement with the theoretical predictions. However, there are issues with the other two modes. The measured rotational mobility is consistently greater than the theory by a factor of ~1.2 – 3, and case of parallel motion is inconclusive due to limitations of the current data collection methods.

5.1 Perpendicular Mobility

To test the case of motion perpendicular to the boundary, I tracked five islands with reduced radii a/l_s ranging from 1.3 to 11.6. In each of these cases, the experimental data closely matched the theoretical curve along the full range of measured distances, as shown in Figure 16.

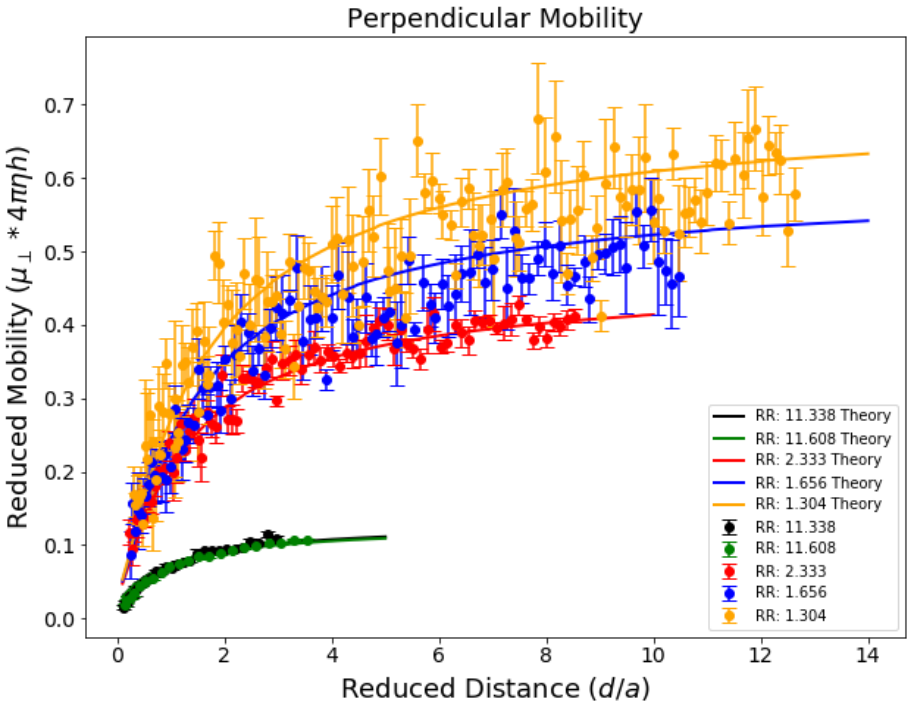

Figure 16: Reduced perpendicular translational mobility vs. reduced distance with theoretical predictions for islands of different reduced radii (RR).

In figure 16, the larger islands can be tracked over a smaller range of distances because they take up more space in the video frame, and thus leave the frame sooner than smaller islands. The error bars are larger for smaller islands because the gravitational force and induced velocity is smaller for these islands, meaning the random Brownian motion contributes more.

5.2 Parallel Mobility

The current experimental procedure I am using introduces a limitation to collecting data for mobility parallel to the film boundary; namely, since the inclusion is moving parallel to the boundary, the island's distance from the boundary changes very little. During this time, the island is also shrinking. After a short time, the island's radius has changed enough that it requires a recalculation of the theory since the theory depends on radius. This means that it is difficult to collect data that spans a large range of distances for a given island radius, and the data points are sparse, as seen in Figure 17.

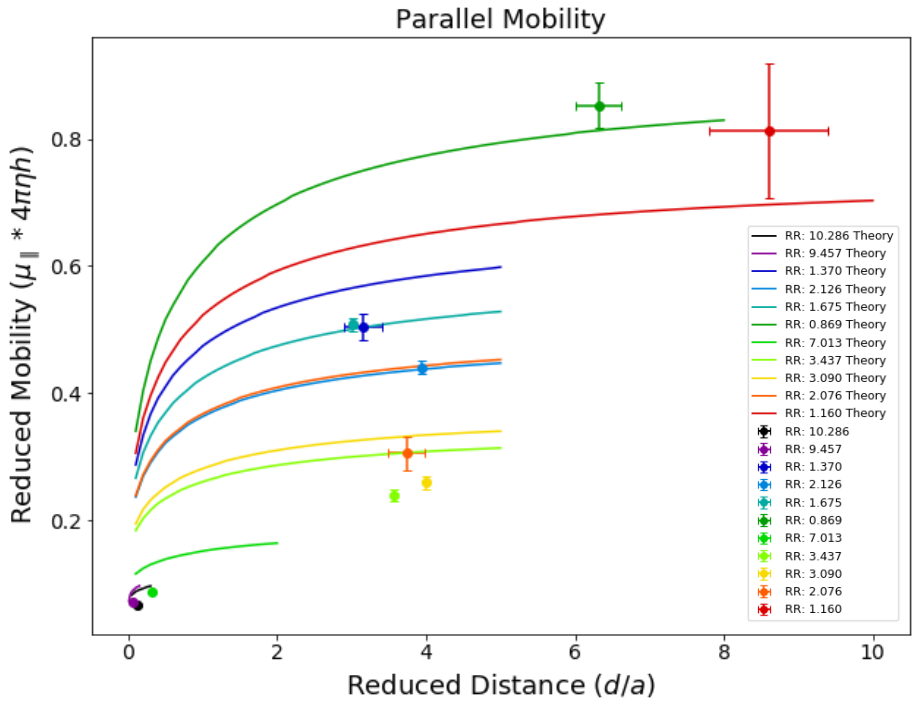

Figure 17: Reduced parallel mobility for islands of many different reduced radii (RR). The color of the theory lines matches that of the data points they correspond to.

I was unable to obtain many points near to the boundary, where the theoretical shoulder is. The agreement with theory is only moderately good. The case of the parallel mode is an area where great improvements could be made to the data collection methods, such as perhaps inducing some perpendicular motion as well to vary the island's distance from the boundary, or alternatively recording much shorter video clips, then re-adjusting the island's distance.

5.3 Rotational Mobility

Throughout many measurements of the rotational mobility, most of the experimental data shows a reduction in the mobility near the boundary as the theory predicts. However, these data consistently exhibit a larger mobility than predicted, generally by a factor of approximately 1.2 to 3, as shown in Figure 18.

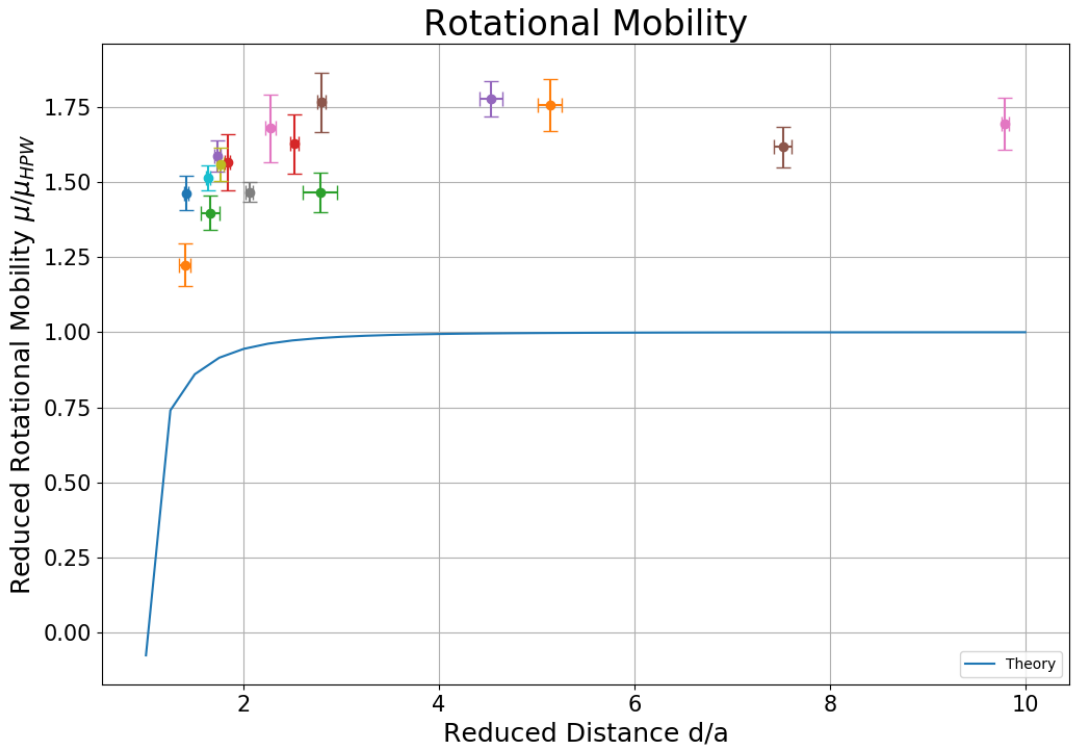

Figure 18: Example of the experimental rotational mobility data. The mobility falls off near the boundary, but the magnitude of the mobility is consistently greater than predicted by theory. In this case, $a / l_s = 1.19$

The cause of this discrepancy is currently unknown. There are multiple potential causes for this discrepancy such as: introducing the ash particles somehow increases the mobility of islands on the film; the ash particles are not stuck to the island boundary, but are diffusing along the boundary; there is an issue with my data analysis; and that there is some physical process occurring that is not being taken into account in the theory.

To test whether the ash particles change the mobility of islands, I analyzed the translational diffusion of an island far from the boundary on a level film. This was done both with and without ash, using the same MSD method as for rotation. The results, as shown in Figure 19-a, indicate that translational mobility is unaffected by the introduction of ash onto the film. The same analysis, done for rotational mobility of islands with ash in them, also resulted in data near the HPW theory (Figure 19-b). This is a good indication that the presence of ash in the film does not alter the mobility of islands.

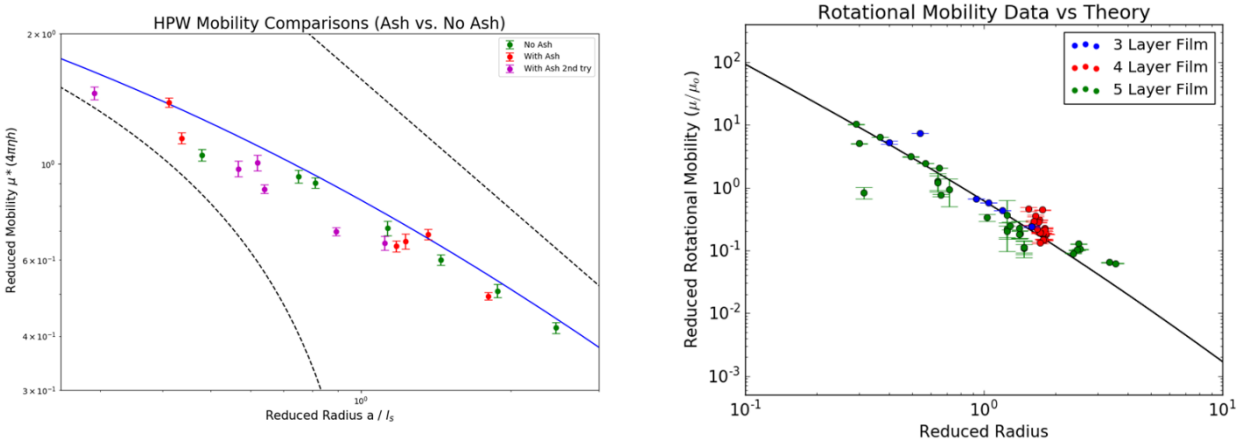

Figure 19: (a): Translational mobility of islands with negligible gravitational drift and far from the boundary, both with and without ash on the film. (b): measurements of rotational mobility far from the boundary on a level film.

At one point while making a film and depositing ash onto it, oval-shaped islands formed, like the one in Figure 20. The island orientation was measured by fitting an ellipse to them, eliminating the need to track particles within the island. The non-isotropic shape of these islands means that the theoretical predictions must be altered. However, in discussions with Tatiana

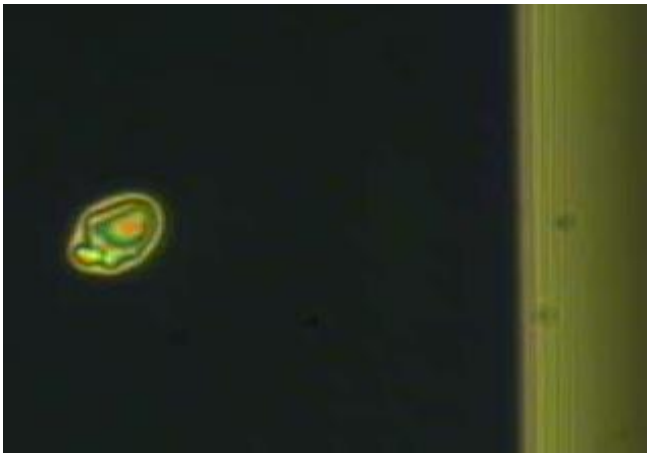

Figure 20: Oval island near the meniscus. This island had a slight drift toward the meniscus while its rotation was tracked.

Kuriabova we found that the new theory was very similar to that of a circular island for the island sizes we measured. The results of this test, however, still showed an average rotational mobility greater than predicted (Figure 21).

This result suggests that the issue does not lie in any diffusion of the ash particles within the island. The issue is perhaps due to faulty analysis of the data, or possibly due to an incomplete theory; for instance, it may be possible that the rotational mobility is coupled to the translation of the island, a phenomenon that is not included in the current theory.

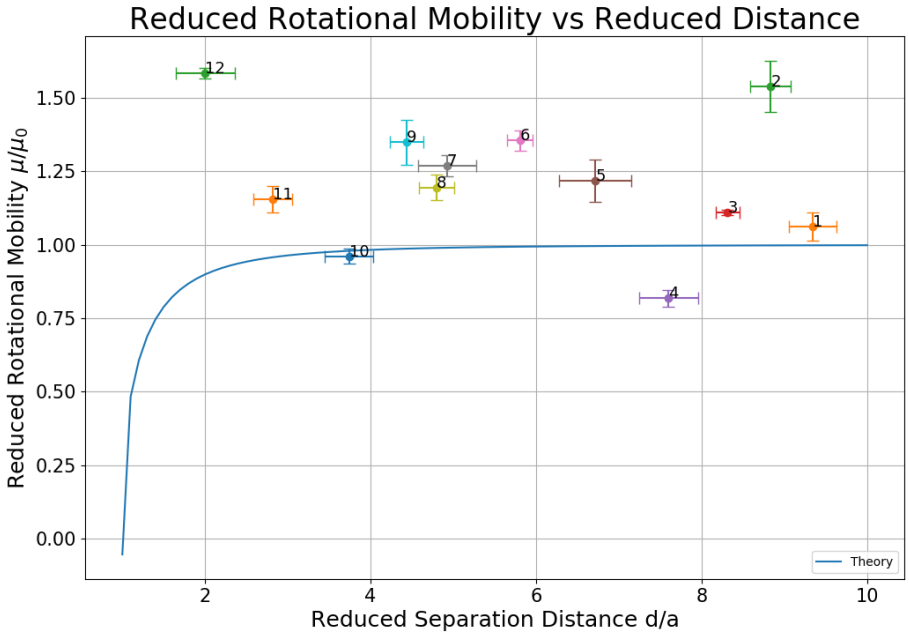

Figure 21:The rotational mobility of the oval island shown above. No boundary effect is present and the average rotational mobility is greater than the predicted value.

Chapter 6

Conclusions and Future Work

The experimental data for each of the modes of diffusive motion agree the theory to varying degrees. The data for the perpendicular mobility agrees almost exactly with the model for a range of island sizes and distances. The parallel and rotational mobilities were not as successful: the parallel mode lacks sufficient data to make conclusions, and the rotational mode shows systematic disagreement with the model despite following the same trend.

Future work on this subject should address two main issues: collecting more data for the parallel mode, and determining the cause of the greater mobility seen in the rotational mode. To collect more data for the parallel mode, it may be possible to give the island a drift that moves it simultaneously parallel and perpendicular to the boundary. The purely perpendicular mode has been shown to agree with the model, so this can provide a test of the effectiveness of this approach: if the mobility perpendicular to the boundary still agrees with the model under this mixed motion, then it can be assumed that the parallel and perpendicular modes remain distinct in this situation.

There are many potential causes of the greater rotational mobility. It is possible that the ash particles raise the temperature of the film, which would also change its viscosity. Another possibility is that there may be an issue with the methods we used to analyze the data for rotation. Finally, it may be that the 8CB sample has been contaminated, which can also change the film properties.

Once these issues have been eliminated and experimental data matches theory for each of these modes, and it would be interesting to extend this theory to irregularly-shaped inclusions, such as would be found in a biological membrane.

References

[1] P. G. Saffman and M. Delbrȍck, “Brownian motion in biological membranes,” Proc. Nat. Acad. Sci. USA, vol. 72, pp. 3111-3113, 1975.

[2] P. G. Saffman, “Brownian motion in thin sheets of viscous fluid,” J. Fluid Mech., vol. 73, pp. 593-602, 1976.

[3] Z. H. Nguyen et al., “Crossover between 2D and 3D fluid dynamics in diffusion of island in ultrathin freely suspended smectic films,” Phys. Rev. Lett., vol. 105, p. 268304, 2010.

[4] C. Klopp, R. Stannarius, and A. Eremin, “Brownian dynamics of elongated particles in a quasi-two-dimensional isotropic liquid,” Phys. Rev. Fluids, vol. 2, p. 124202, 2017.

[5] P. Pieranski et al., “Physics of smectic membranes,” Physica A, vol. 194, pp. 364-389, 1993.

[6] S. P. Radzihovsky et al., “Two-dimensional island emulsions in ultrathin, freely-suspended smectic liquid crystal films,” Soft Matter, vol. 13, pp. 6314-6321, 2017.

[7] D. Davidov et al., “High-resolution x-ray and light-scattering study of critical behavior associated with the nematic—smectic-A transition in 4-cyano-4′-octylbiphenyl,” Phys. Rev. B, vol. 19, pp. 1657-1663, 1979.

[8] A. J. Leadbetter, J. L. A. Durrant, and M. Rugman, “The density of 4 n-octyl-4-cyano-biphenyl (8cb),” Molecular Crystals and Liquid Crystals, vol. 34, pp. 231-235, 1976.

[9] F. Schneider, “Measurement of the viscosity coefficient η3 in free-standing smectic films,” Phys. Rev. E, vol. 74, p. 021709, 2006.

[10] P. E. B. Weast and R. C., Handbook of Chemistry and Physics-54th Edition, vol. 1. CRC Press, Cleveland, 1973.

[11] P. Oswald and P. Pieranski, Smectic and Columnar Liquid Crystals: Concepts and Physical Properties Illustrated by Experiments, vol. 1. CRC Press, 2005.

[12] E. P. Petrov, R. Petrosyan, and P. Schwille, “Translational and rotational diffusion of micrometer-sized solid domains in lipid membranes,” Soft Matter, vol. 9, pp. 7552–7555, 2012.

[13] R. Brown, The Miscellaneous Botanical Works of Robert Brown, vol. 1. R. Hardwicke, London, 1866.

[14] A. Einstein, “Über die von der molekularkinetischen Theorie der Wärme geforderte Bewegung von in ruhenden Flüssigkeiten suspendierten Teilchen,” Annalen der Physik, vol. 322, pp. 549-560, 1905.

[15] M. von Smoluchowski, "Zur kinetischen Theorie der Brownschen Molekularbewegung und der Suspensionen". Annalen der Physik, vol. 21, pp. 756-780, 1906.

[16] B. D. Hughes, B. A. Pailthorpe, and L. R. White, “The translational and rotational drag on a cylinder moving in a membrane,” J. Fluid Mech., vol. 110, pp. 349-372, 1981.

[17] G. G. Stokes, “On the effect of the internal friction of fluids on the motion of pendulums,” Cambridge Philos. Trans., vol. 3, p. 8106, 1851.

[18] E. P. Petrov and P. Schwille, “Translational Diffusion in Lipid Membranes beyond the Saffman-Delbrück Approximation,” Biophys. J., vol. 94, pp. L41-L43, 2008.

[19] A. J. Levine and F. C. MacKintosh, “Dynamics of viscoelastic membranes,” Phys. Rev. E vol. 66, p. 061606, 2002.

[20] A. J. Levine, T. B. Liverpool, and F. C. MacKintosh, “Mobility of extended bodies in viscous films and membranes,” Phys. Rev. E vol. 69, p. 021503, 2004.

[21] T. Kuriabova et al., “Hydrodynamic Interactions in Freely Suspended Liquid Crystal Films,” Phys. Rev. E, vol. 94, p. 052701, 2016.

[22] C. Rosenblatt and N. M. Amer, “Optical determination of smectic A layer spacing in freely suspended thin films,” Appl. Phys. Lett., vol. 36, p. 432, 1980.

[23] J. C. Crocker, D. G. Grier, “Methods of Digital Video Microscopy for Colloidal Studies,” J. Colloid Interface Sci., Volume 179, pp. 298-310, 1996.